Approach of semi-infinite dynamic lattice Green's function and energy dissipation due to phonons in solid friction between commensurate surfaces

Seiji Kajita, Hitoshi Washizu, and Toshihide Ohmori
Toyota Central R&D Labs., Inc., 41-1, Yokomichi, Nagakute, Nagakute-cho, Aichi 480-1192, Japan
(Received 26 April 2010; revised manuscript received 23 July 2010; published 14 September 2010)

To investigate the relationship between solid friction and energy dissipation due to phonon, we developed a coupled-oscillator surface model that consists of an infinitely large number of bulk atoms in a solid. This method is formulated using a dynamic lattice Green's function. A self-consistent scheme used for achieving a steady state and a fast convolution method that reduces the high computational overhead are also presented. Furthermore, a methodology to decompose the friction coefficient with the surface phonon modes is obtained. The energy absorption band corresponding to the wave number of the surface phonon is found. These approaches clarify the role of the energy-dissipation mechanism in sliding friction. Two-dimensional friction models in which both surfaces have same lattice constant, i.e., commensurate surfaces, are used to demonstrate these methods. In the analysis of a friction system between flat surfaces, energy transfer from the kinetic energy of a sliding solid to low-frequency surface phonons in the counter solid occurs in the presence of bulk atoms. The energy dissipation into the bulk system leads to friction. We also investigate a friction system between periodically contacting surfaces. It is found that surface phonons with nonzero wave number act as channels for energy dissipation and alter the friction profile depending on the size of the contact area. When the contact size is so large that a sufficient number of the nonzero wave number modes act as the energy-dissipation channels, the profile of the friction decomposition with the nonzero wave number modes exhibits good agreement with that estimated by a simple continuum model.

DOI: 10.1103/PhysRevB.82.115424 PACS number(s): 68.35.Af, 46.55.+d, 81.40.Pq

I. INTRODUCTION

Technologies to control friction are essential requirements in order to solve environmental issues and realize a zero-emission society by reducing energy consumption. In the past, the technical improvements have been done by using knowledge obtained from elastic-contact theory, hydrodynamics, and chemical analysis.[1–3] For example, the theory of hydrodynamic lubrication based on the Reynolds equation enables one to expect friction properties in the range of hydrodynamic lubrication.[4,5] Furthermore, recent developments of contact theory between solids provide qualitative explanations of solid friction behavior.[2,3,6–12] However, some important issues such as expectation of friction coefficient in ranges of boundary and mixed lubrication involving solid contact have not been clarified yet.

One of the main difficulties in solid friction stems from the fact that the friction is affected by various scale processes: atomic-scale process such as collision of surface atoms and chemical reactions, and macroscale ones such as plastic deformation and production of wear debris.[2,13,14] Another reason is the fact that friction is a dynamic phenomenon. Because *in situ* observation of a rubbing interface is extremely difficult, we must rely on measurements of a rubbed surface after sliding. Additionally, the construction of a theory to treat dynamical phenomena emerging during energy dissipation, namely, nonequilibrium steady states, still remains a major challenge in the sphere of theoretical physics[15]

However, recent analysis techniques, e.g., atomic force microscopy,[16] and simulation methods such as molecular-dynamics (MD),[17–28] and electronic state calculations[29] have been employed to investigate the microscopic elementary processes that could not be studied previously; they have greatly contributed toward gaining basic understanding of solid friction[13,14] The two constituent factors of solid friction can be categorized as follows: (a) interface phenomena: surface electronic state, adsorbate, lubricant molecule, plastic deformation, adhesion, wear, etc. (b) Energy dissipation mechanism of a solid: excitations of phonon (general solids) and electron (mainly metals).

Because contact areas during friction can be intense reaction fields due to the high local pressure and shear stress, many studies have focused on the relationship between the interface phenomena and the friction. On the other hand, the energy dissipation mechanism of a solid depends on the bulk property. The kinetic energy of a sliding solid triggers the interface phenomena that induce excitations of the inner degrees of freedom of a solid; in the case of a phonon, for instance, lattice vibrations (phonons) are excited. The excited phonons propagate into an inner solid and convert into thermal energy, and thus, they never return to the surface unless impurities exist in the solid. The irreversible processes lead to energy loss, i.e., friction. Therefore, the study of friction should be addressed in detail from the viewpoint of the energy dissipation mechanism of a solid as well as the interface phenomena. However, owing to the difficulty of dealing with such a highly nonequilibrium phenomenon, the relationship between the friction and the energy dissipation mechanism has not yet been clarified well. Our work focuses on the energy dissipation due to a phonon because it plays the role in general solids.

One of the solutions for depicting the energy dissipation mechanism of a solid is to include infinitely large bulk atoms of a solid. Suppose that in a finite-sized solid an impinged surface phonon reaches the bottom of the solid and reflects to

the surface; this cannot be irreversible process. If we can project degrees of freedom of infinitely large atoms into the coordinates of the surface atoms, the surface atoms are damped by a damping kernel that represents phonon energy dissipation without reflection; this projection directly yields the framework of the generalized Langevin equation.[30,31] Zwanzig[32] first used the projection in a one-dimensional harmonic chain model to analyze gas collision on a solid surface. In order to include the temperature effect, Adelman and Doll[33,34] generalized the formulation within the generalized Langevin approach and showed that the damping kernel can be connected to the lattice Green's function (LGF) that expresses the response of a system with external force.[35,36] Some extensions of this approach have been done for the purpose of developing multiscale strategies that couple together atomistic and continuum numerical methods.[37–41]

In keeping with the trend of the LGF method, Campañá and Müser[42] developed an MD simulation method based on static LGF of elastic semi-infinite solids for the static and quasistatic friction analysis. For the dynamic system, Sokoloff[43,44] first investigated the kinetic friction in a one-dimensional chain system by applying perturbation theory to dynamic LGF. Recently, Braun *et al.*[45] constructed the nonperturbative dynamic LGF of the same system in the Fourier-frequency space in order to study the transition of stick-slip motion.[45] Their approach, however, considers the atomic coordinates only in the one-dimensional direction: sliding direction. In our previous work,[46] we formulated the dynamic LGF of the one-dimensional chain system in real-time space extending two-directional degrees of freedom: sliding and surface normal directions. This extension enables us to obtain the kinetic friction coefficient because the normal pressure can be defined explicitly. We revealed a significant dependence of the friction coefficient on the properties of the inner bulk atoms.

To the best of our knowledge, despite its potential effectiveness for various physical phenomena, there are few works using the semi-infinite dynamic LGF (SI-DLGF) other than a simple system such as a one-dimensional harmonic chain. One of the impediments in its use is that deriving analytical solutions of the SI-DLGF above one-dimensional system is difficult although some numerical approaches for tackling this problem have recently been reported.[38–41] Another difficulty is the computational costs. It is well known that the ordinary numerical treatment for the convolution that appears in the SI-DLGF formalism has a high computational cost because the calculation requires the past history of the phenomenon.

In this work, we propose the SI-DLGF for a harmonic two-dimensional square lattice system, which is derived analytically. This formulation easily extends to the three-dimensional cubic one. The advantage is that this method treats the infinitely large number of solid atoms that cannot be treated by conventional MD simulations. Furthermore, using the analyticity of the SI-DLGF, we introduce a fast convolution method[47–50] that reduces the high computational costs dramatically. These findings enable the SI-DLGF method to be applied to a large and general system. We also present a method for the decomposition of the friction coefficient in wave numbers and frequencies of surface phonon modes. The method tells us the contribution of each surface phonon mode to the total friction coefficient; it is useful to analyze the solid friction in terms of the dynamics of surface atoms. The SI-DLGF and the friction decomposition methods will be demonstrated using simple two-dimensional friction systems in which both surfaces have same lattice constant, commensurate surfaces in other words. Although the commensurate systems artificially enhance elastic instability that does not make such a large contribution to realistic friction,[21–24,51,52] we intentionally use the systems for the purpose of a fundamental study of the phonon dissipation in the solid friction.

In these methods, we assume that the intrabonds in a solid are replaced with springs connected to the nearest-neighbor atoms. The effect of anharmonicity cannot be included. Furthermore, the methods are restricted to the square and cubic structures and single constitution of atomic elements. Therefore, our methods should be used to acquire a basic understanding of the role of the energy-dissipation mechanism due to phonons in solid friction, rather than a quantitative analysis that can be carried out by atomic-scale simulations such as MD and electronic state calculation.

This paper is organized as follows. Section II provides theoretical descriptions of the SI-DLGF, the fast convolution, and the friction decomposition method, and the computational details are shown in Sec. III. The SI-DLGF results of two simple friction systems are presented in Sec. IV. One analysis is performed in a friction system between flat surfaces, which completes our previous study of the same system.[46] Another analysis is performed using a system that contains periodic contact areas. Through these results, we discuss the relationship between surface dynamics and solid friction. Section V provides the summary and conclusion.

II. FORMULATION

We present descriptions of the theoretical approach. Although the formulation is provided for a two-dimensional square lattice, all the methodologies in this section can be extended to a three-dimensional cubic lattice through a similar procedure.

A. Surface lattice model

We consider a two-dimensional square lattice in which N and N' atomic layers align in the surface normal direction (z) and lateral direction (x), respectively. The bottom layer connects to a rigid body. Applied periodic boundary condition in the x direction, the lattice forms a surface. We assume that bonds between atoms in the solid are replaced with springs and only the surface atomic layer is subjected to external force. We denote the x and z displacements of an atom by u, and the equation of motion of the lattice is then given by

$$m\ddot{u}_{\eta,\xi} + K_u\left(2u_{\eta,\xi} - \sum_{\Delta\xi} u_{\eta,\xi+\Delta\xi} - \delta_{\xi,1}u_{\eta,1}\right) + K'_u\left(2u_{\eta,\xi} - \sum_{\Delta\eta} u_{\eta+\Delta\eta,\xi}\right) = \delta_{\xi,1}F^u_\eta, \quad (1)$$

where atomic labels η and ξ are $\eta = 1,2,\ldots,N'$ and ξ

$=1,2,\ldots,N$, respectively. $\xi=1$ represents a surface atomic layer and $\xi=N$ is a bottom atomic layer connected to a rigid body. δ and Δ denote the Kronecker delta and nearest-neighbor atomic label, respectively. m and F are an atomic mass and external interaction force. Although the interaction force is a function of time t and atomic positions $\mathbf{r}(t)$, we denote it by simply $F(t)$ as long as no ambiguity arises. $K_u^{(\prime)}$ is a spring constant of a bond between atoms labeled by the neighboring $\xi(\eta)$. Owing to the periodic boundary condition in the x direction, u satisfies $u_{\eta,\xi}=u_{\eta+N',\xi}$.

We rewrite Eq. (1) in the tensor expression as

$$\left(\frac{d^2}{dt^2}+\hat{D}+\hat{D}'\right)\begin{pmatrix}\mathbf{u}_1\\ \mathbf{u}_2\\ \vdots\\ \mathbf{u}_\xi\\ \vdots\\ \mathbf{u}_N\end{pmatrix}=\begin{pmatrix}\mathbf{F}^{\mathbf{u}}/m\\ 0\\ \vdots\\ \vdots\\ \vdots\\ 0\end{pmatrix}, \tag{2}$$

$$\mathbf{u}_\xi=(u_{1,\xi},u_{2,\xi},\ldots,u_{\eta,\xi},\ldots,u_{N',\xi}),$$

where $\hat{D}$ and $\hat{D}'$ represent the elastic force between atoms corresponding to the second and third term on the left-hand side in Eq. (1), respectively. We use the accented mark $\hat{}$ to indicate the fourth rank tensor of $N\times N\times N'\times N'$ in the following.

B. Semi-infinite dynamic lattice Green's function

The Green's function of Eq. (2) satisfies the following equation:

$$\left(\frac{d^2}{dt^2}+\hat{D}+\hat{D}'\right)\hat{G}(t)=\hat{I}\delta(t),$$

$$\hat{G}(t=0)=\frac{d}{dt}\hat{G}(t=0)=0,$$

where $\hat{I}$ is a unit tensor. By Laplace transformation, we obtain

$$(\bar{z}^2+\hat{D}+\hat{D}')\hat{G}(\bar{z})=\hat{I}, \tag{3}$$

where $\bar{z}$ is a complex coordinate. Then, we operate diagonal matrices $\hat{U}^D$ and $\hat{U}^{D'}$ for $\hat{D}$ and $\hat{D}'$ on Eq. (3). Using the facts that $\hat{U}^D$ and $\hat{U}^{D'}$ commute and that their tensor elements are $U^D_{\eta,\xi,l,j}=\delta_{\eta,l}U^D_{\xi,j}$ and $U^{D'}_{\eta,\xi,l,j}=\delta_{\xi,j}U^{D'}_{\eta,l}$, we obtain

$$[\hat{U}^D\hat{U}^{D'}\hat{G}(\bar{z})]_{\eta,\xi,l,j}=\frac{U^D_{\xi,j}U^{D'}_{\eta,l}}{\bar{z}^2+(\omega_j^D)^2+(\omega_l^{D'})^2}, \tag{4}$$

where $(\omega_j^D)^2$ and $(\omega_l^{D'})^2$ are the eigenvalues of $\hat{D}$ and $\hat{D}'$, respectively. Then, we operate $(\hat{U}^D)^{-1}$ and $(\hat{U}^{D'})^{-1}$ and perform the inverse Laplace transform. Note that $\hat{U}^D$ and $\hat{U}^{D'}$ are unitary matrices. Here, we treat the time derivative of $\hat{G}$ rather than $\hat{G}$ itself for the sake of convenience in the following formulations. The matrix element of $\hat{g}=d/dt\hat{G}$ in $t>0$ is given by

$$g_{\eta,\eta',\xi,\xi'}(t)=\sum_{j,l}U^D_{\xi,j}U^D_{\xi',j}U^{D'}_{\eta,l}U^{D'}_{\eta',l}\cos(\sqrt{(\omega_j^D)^2+(\omega_l^{D'})^2}t). \tag{5}$$

ω_j^D, $\omega_l^{D'}$, U^D_j, and $U^{D'}_{\eta,l}$ can be written as

$$\omega_j^D=\alpha\sin\theta_j,\quad \omega_l^{D'}=\alpha'\sin Al/2,$$

$$U^D_{\xi,j}=\{\sin 2\xi\theta_j-\sin 2(\xi-1)\theta_j\}/(\sqrt{2N+1}\sin\theta_j),$$

$$U^{D'}_{\eta,l}=\{\cos Al(\eta-1)+\sin Al(\eta-1)\}/\sqrt{N'},$$

where $\theta_j=\pi(j-1/2)/(2N+1)$, $\alpha^{(\prime)}=2\sqrt{K_u^{(\prime)}/m}$, and $A=2\pi/N'$. $j=1,2,\ldots,N$, and $l=0,\pm1,\pm2,\ldots,\pm(N'/2-1),N'/2$ in the case of even N' and $l=0,\pm1,\pm2,\ldots,\pm(N'-1)/2$ in the case of odd N'. Because the interaction force affects only the surface atomic layer $\xi=1$, the tensor element of $\hat{g}$ that we need to consider is $\xi'=1$. Furthermore, it is sufficient to know the motion of the surface atomic layer for the purpose of the friction analysis; thus, we only consider $g_{\eta,\eta',\xi=1,\xi'=1}$ hereafter, omitting the indices ξ and ξ' for the sake of simplicity. Substituting the above-mentioned eigenvalues and matrix elements into Eq. (5) gives

$$g_{\eta,\eta'}(t)=\frac{1}{N'}\sum_l\cos Al(\eta-\eta')s_l(t), \tag{6}$$

$$s_l(t)=\sum_j\frac{4}{2N+1}\cos^2\theta_j\cos(\alpha\sqrt{\sin^2\theta_j+\beta_l^2}t),$$

where $\beta_l=\sqrt{K_u'/K_u}\sin Al/2$. In the limit of infinite N, we can convert the summation of s_l into an integral changing variable $\theta_j\to\theta$ and derive

$$s_l(t)=\frac{4}{\pi}\int_0^{\pi/2}\cos^2\theta\cos(\alpha\sqrt{\sin^2\theta+\beta_l^2}t)d\theta. \tag{7}$$

By the Green's function, the formal solutions of the velocities of the surface atoms can be formulated as

$$\dot{u}_\eta(t)=\dot{u}^0(t)+\sum_{\eta'=1}^{N'}\int_0^t g_{\eta,\eta'}(t-t')F^u_{\eta'}(t')/mdt', \tag{8}$$

where $\dot{u}^0$ is the solution under an initial condition in which the lattice distorts uniformly without any external force. This solution is necessary to obtain the steady state of the friction system; we will discuss about it in the next subsection. Although Eq. (8) is the basic equation, it requires N'^2 number of convolutions if we use Eq. (8) itself for the simulations. For the sake of reduction of the number of convolution to be N', we rewrite the solution substituting Eq. (6) into Eq. (8) as

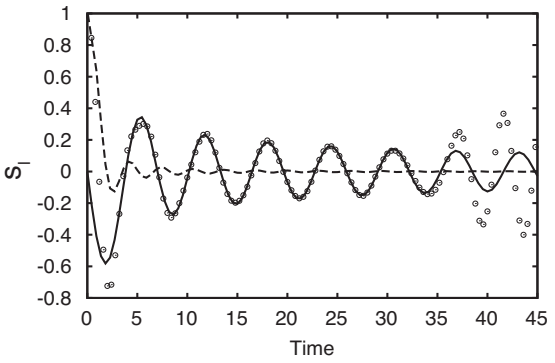

FIG. 1. Profiles of the SI-DLG F. White circles, solid line, and dashed line indicate s_l obtained by the numerical θ integration in Eq. (7), the asymptotic solution $\tilde{s}_l$ [Eq. (13)], and s_0 [Eq. (12)]. $\alpha=2$, $\beta_l=0.5$, and the partition number of the θ integral is 13.

$$\dot{u}_\eta(t) = \dot{u}^0(t) + \sum_l \int_0^t s_l(t-t')\{F_l^{uc}(t')\cos Al\eta + F_l^{us}(t')\sin Al\eta\}dt'/m, \tag{9}$$

where $F_l^{uc}=\Sigma_{\eta'}F_{\eta'}^u/N'\cos Al\eta'$ and $F_l^{us}=\Sigma_{\eta'}F_{\eta'}^u/N'\sin Al\eta'$. The meaning of s_l becomes clear by the discrete Fourier transformation of $\dot{u}_\eta$: $\dot{u}_l=1/N'\Sigma_{\eta=1}^{N'}\exp(iAl\eta)\dot{u}_\eta$. Equation (9) transforms into

$$\dot{u}_l(t) = \delta_{l,0}\dot{u}^0(t) + \int_0^t s_l(t-t')F_l^u(t')dt'/m, \tag{10}$$

where

$$F_l^u = \frac{1}{N'}\sum_{\eta=1}^{N'}\exp(iAl\eta)F_\eta^u. \tag{11}$$

Namely, s_l represents the SI-DLGF in the wave number l space of the surface lateral direction.

The remaining task is to obtain specific values of s_l. In the case of $l=0$, Eq. (7) can be solved as (see Appendix A)

$$s_0(t) = 2J_1(\alpha t)/(\alpha t), \tag{12}$$

where J_n is the first-kind Bessel function of order n. The profile of s_0 is shown in Fig. 1 (dashed line). On the other hand, $s_{l\neq 0}$ is not expressed explicitly but is formulated by the integral expression in Eq. (7). It should be noted that we must not operate the integral numerically. Let us recall that the integral is originally derived from the conversion of the summation of j in the limit of infinite N. Thus, when the integral is performed by the finite difference method, it amounts to calculating s_l of the finite bulk system corresponding to the partition number of the θ integral. Figure 1 (white circles) shows the result of s_l obtained using the finite difference method. s_l decreases with time. This indicates that the response of an atom with an applied force decays; in other words, a surface phonon excited by an external force diminishes because of the propagation of the wave over the bulk atoms. However, at $t\sim 35$, s_l recovers significant amplitude. This is attributed to the recurrence of a vibration wave that reflects at the bottom of the lattice.

The easiest way to prevent the recurrence of the vibration wave is to take a sufficiently large value of partition number of the θ integral so that the vibration wave does not return in the simulation time. However, the time required for ordinary friction simulations is generally quite long (>100 ps) with respect to the time scale of s_l. Thus, the numerical integration with such a large partition number would become impossible. More critically, this procedure does not adhere to the theoretical framework for the semi-infinite lattice system.

Therefore, in order to involve the infinite bulk atoms, we have to perform the integral in Eq. (7) analytically. Although we could not find the solution of the integral over whole values of t, we found that the integral can be solved in a large t limit and the asymptotic solution of s_l is obtained. The detailed derivation appears in Appendix A. The asymptotic solution $\tilde{s}_l$ is derived as

$$\tilde{s}_l(t) = -2\beta_l J_1(\alpha\beta_l t). \tag{13}$$

Figure 1 (solid line) shows the profile of $\tilde{s}_l$; it decreases with time without the reflection of vibration even in the region of $t>35$. In the small t region, it is seen that $\tilde{s}_l$ immediately converges with the numerically obtained s_l profile. The good convergence performance of the asymptotic solution is attributed to the fact that the asymptotic condition $\int_0^y dyJ_1(y)/y\to 1$ (see Appendix A), where $y=\alpha t/2$, is well satisfied even at a relatively small t region, because the integrand $J_1(y)/y$ decays relatively fast as $t^{-3/2}$.

We offer a strategy to construct s_l. First, set the value of t_c such that the asymptotic solution $\tilde{s}_l$ becomes nearly equal to s_l, which is obtained from Eq. (7) by the numerical method with enough partition number such that the reflection of vibration at t_c does not occur. Then, the numerically obtained s_l is used in $t\leq t_c$ and the asymptotic solution is set in $t>t_c$.

C. Self-consistent scheme to achieve a steady state

We introduced $\dot{u}^0$, the solution of Eq. (2) for $F=0$, under the initial condition in which a uniform distortion is imposed on all atoms in the lattice. The solution is required for achieving a steady state for the infinite N lattice system, because the elastic force of the infinite lattice vanishes in terms of scaling arguments.[46,53] Let us illustrate this fact with the following example.

If all atoms are assumed to have no distortions and are at rest as an initial condition, $u^0(t)$ and $\dot{u}^0(t)$ are zero. Even under the initial condition, in a finite N lattice system, the lattice distorts due to friction and normal forces and the elastic forces of the distortions balance the forces after a certain time period; then, a steady state is achieved. On the other hand, in the case of an infinite N system, it is impossible to attain distortions that balance the friction and normal forces because it takes infinite time to distort the infinite bulk atoms. This fact indicates that we cannot achieve a steady state for the infinite N system if we simply employ the $u^0(t)=\dot{u}^0(t)=0$ solutions.

The problem specific to the infinite N system can be overcome by the initial state providing a uniform distortion over the infinite N atomic layers in advance. Then, the initial distortion is chosen to balance the friction force at the steady

state. Here we derive $\dot{u}^0$ that satisfies the initial condition.

Because the uniform distortions over all the atoms are considered, the elastic-force term resulting from the displacement between atoms labeled by η vanishes. This model is equivalent to a one-dimensional chain system. Thus, with the index η being omitted, the motion equation of the finite N system is written as

$$\ddot{u}^0_\xi + \frac{K_u}{m}\left(2u^0_\xi - \sum_{\Delta\xi} u^0_{\xi+\Delta\xi} - \delta_{\xi,1}u^0_1\right) = 0,$$

$$u^0_\xi(t=0) = A_u(N-\xi+1), \quad \dot{u}^0_\xi(t=0) = 0,$$

where A_u denotes a constant displacement between adjacent atoms; i.e., $u^0_\xi(t=0) - u^0_{\xi+1}(t=0) = A_u$. Multiplying by $U^D_{\xi,j}$ and denoting $\tilde{u}^0_j = \sum_\xi U^D_{\xi,j} u^0_\xi$, we obtain

$$\left\{\frac{d^2}{dt^2} + (\omega^D_j)^2\right\}\tilde{u}^0_j = 0.$$

This equation can be solved as $\tilde{u}^0_j(t) = c_j \cos \omega^D_j t$. The undetermined coefficient c_j is derived from the initial condition as

$$c_j = A_u \sum_{\xi=1}^{N} (N-\xi+1) U^D_{\xi,j} = \frac{A_u}{2\sqrt{2N+1}} \frac{\cos\theta_j}{\sin^2\theta_j}$$

and $u^0_\xi(t)$ is expressed as

$$u^0_\xi(t) = \sum_{j=1}^{N} U^D_{\xi,j} c_j \cos \omega^D_j t.$$

In the same manner as that in the last subsection, we only consider $\xi=1$, and omit the index. Taking the limit of infinite N, the time derivative of u^0 can be derived as

$$\dot{u}^0(t) = \frac{-A_u\alpha}{2}\left\{J_1(\alpha t) + \alpha\int_0^t J_2(\alpha t)dt\right\}, \tag{14}$$

where integral expressions of the Bessel functions were used.

Let us emphasize that A_u are important parameters because they control the force balances of the system along the x and z directions in the steady state. In the z direction, the parameter A_z gives a compression along the surface normal direction over an infinitely large bulk system. One can determine an averaged normal force per atom $\bar{F}^z$ in a given friction system by choosing $A_z = \bar{F}^z/K_z$. The parameter A_x, in turn, represents the distortion along the shear direction, and it is not decided a priori like A_z. Next, we present a scheme to obtain A^*_x that achieves a steady state. Because $\langle \dot{x}_\eta \rangle_t$ is zero at the steady state, we can derive the condition of A^*_x using Eqs. (7), (9), and (14)

$$A^*_x = \frac{1}{K_x}\left\langle \sum_{\eta=1}^{N'} F^x_\eta(\{\mathbf{r}_\eta\},t)/N' \right\rangle_t, \tag{15}$$

where $\langle\rangle_t$ denotes a long-time-averaged operation and $\{\mathbf{r}_\eta\}$ represents a set of atomic coordinates of the surface atoms.

The specific steps for achieving a steady state in the SIDLGF method are as follows. (i) Set a sliding velocity, A_z that determines the normal pressure, and an arbitrary value of A_x. Then, calculate the time evolution of the surface atoms by Eq. (9). (ii) Insert the calculated $\{\mathbf{r}_\eta\}$ into the right-hand side of Eq. (15). The obtained value is denoted by A'_x. (iii) If $|(A'_x - A_x)/A_x| = \delta A_x > \Delta$, it is judged that A_x used in the calculation does not give the steady state, where Δ is a small value. Then, replace $\epsilon A'_x + (1-\epsilon)A_x \to A_x$ and return to step (i), where $0 < \epsilon < 1$. If $\delta A_x < \Delta$, it is judged that $A_x = A^*_x$ and the steady state is realized.

This scheme is a self-consistent calculation for finding A^*_x. Owing to the iteration of steps (i)–(iii), we can achieve a steady state for the infinite N friction system and obtain the friction coefficient.

D. Fast convolution method

Equation (9) involves a convolution of s_l with a force. It is known that a classical method for computing the convolution over N_t time steps requires a large memory space $O(N_t)$ to store a force history and $O(N_t^2)$ operations. The high computational costs impede numerical simulations employing the Green's function approach. In actual simulations, the truncation of time history in the convolution integral is often used. This truncation is applicable if the Green's function, i.e., the response kernel, decreases rapidly with time. In our case, s_0 decays as $t^{-3/2}$ whereas $s_{l\neq 0}$ has a long tail as $t^{-1/2}$. It appears to be necessary to integrate over a long past history in order to maintain the accuracy of the calculations. The fast convolution algorithm using the inverse Laplace transform, called modified Talbot's method, can be a powerful tool in our approach to reduce the computational costs. We present a brief description of this method in the use of our method; the complete description is available in literature.[47–50]

Using the asymptotic solution $\tilde{s}_l$ described in Eq. (13), the convolution can be separated at time point t_c that one chooses so as to suitably converge $\tilde{s}_l$ with s_l. This convolution is approximated when $t > t_c$ as

$$\int_{t-t_c}^{t} \Delta s_l(t-t')F(t')dt' + \int_0^t \tilde{s}_l(t-t')F(t')dt', \tag{16}$$

where F is an arbitrary force function and $\Delta s_l = s_l - \tilde{s}_l$. The first term does not have a high computational cost even if we use an ordinal numerical method because $\tilde{s}_l$ converges to s_l with relatively small t_c. Most of the computational cost arises from the second term because it contains the entire past history of the phenomenon.

In the fast convolution method, the analytical form of the Laplace transform of the kernel is required. We obtained $\tilde{s}_l$ explicitly and its Laplace formation can be written as

$$\tilde{s}_l(\bar{z}) = -2\frac{\sqrt{\bar{z}^2 + (\alpha\beta_l)^2} - \bar{z}}{\alpha\sqrt{\bar{z}^2 + (\alpha\beta_l)^2}},$$

where $\bar{z}$ is a complex coordinate. Then, the time region of the convolution of the second term in Eq. (16) is decomposed. We consider P as the smallest integer for which $t < 2B^P h$, where the base $B > 1$ is an integer, and determine the integer q_p such that $\tau_p = q_p B^l h$ satisfies

$$t - \tau_p \in [B^p h, (2B^p - 1)h], \quad p = 1, \ldots, P-1,$$

where h is an interval of a time step. We set $t=\tau_0>\tau_1>\tau_2>\cdots>\tau_P=0$. With a series of τ_p, the second term of Eq. (16) can be split as

$$\int_0^t \tilde{s}_l(t-t')F(t')dt' = \sum_{p=1}^{P} \int_{\tau_p}^{\tau_{p-1}} \tilde{s}_l(t-\tau)F(\tau)d\tau.$$

Using the inverse Laplace transform, $\int_{\tau_p}^{\tau_{p-1}} \tilde{s}_l(t-\tau)F(\tau)d\tau$ can be written as

$$\mathcal{L}^{-1}\left\{ \tilde{s}_l(\bar{z}) \int_{\tau_p}^{\tau_{p-1}} \exp(-\bar{z}\tau)F(\tau)d\tau \right\}, \tag{17}$$

where $\mathcal{L}^{-1}$ is the operator of the inverse Laplace transform. It is known that the time integral in Eq. (17) can be calculated using the knowledge of $F(\tau)$ and $F(\tau-h)$ recursively:[47,50] thus, we do not have to track the entire history of the force.

The main difficulty in Eq. (17) arises from the numerical integration for the inverse Laplace transform. The integration over Im $\bar{z}=-\infty$ to ∞ causes the oscillation of the exponential $\exp(\bar{z}t)$. In the modified Talbot's method,[47,48,50] the difficulty is solved by replacing the integral line along the complex axis vertically with an integral contour: its start and end points are set at Re $\bar{z}=-\infty$ and the path runs around the singularities of the kernel in a counterclockwise direction. In this manner, the exponential rapidly decays along the contour when we use the finite-difference method on the contour. The choice of the shape of the contour has been determined on the each time region $[\tau_p, \tau_{p-1}]$ experimentally by minimizing the error of the inverse Laplace transform.[47] By using the fast convolution method, the computational costs of the convolution of the second term in Eq. (16) can be significantly reduced: $O(\log_B N_t)$ memory requirement and $O(N_t \log_B N_t)$ operations.

E. Friction decomposition with surface phonon modes

Because energy loss accompanies the energy transformation of the kinetic energy of a sliding solid into the vibration energy of the surface atoms, it is expected that the contribution of the surface phonon to the energy loss generally depends on the phonon modes. Braun *et al.*[45] proposed a method to decompose friction into the contributions of the frequency modes in the semi-infinite one-dimensional chain system. Here, we extend their method of the friction decomposition to the semi-infinite surface system.

Suppose that a body on a surface is sliding at velocity V under normal load F_P. For the sake of conciseness in the following discussion, we assumed that the upper body is rigid and only the lower body is responsible for the energy dissipation. This restriction does not change the following discussion essentially and it can be easily removed. The friction coefficient μ has a thermodynamic relationship with the energy loss rate per unit time J as[2]

$$\mu = \frac{J}{F_P V}. \tag{18}$$

From the microscopic view points, the energy loss rate can be defined by denoting the velocity of a surface atom $\dot{\mathbf{u}}$ in the lower body and force imposed on the surface atoms from the upper body $\mathbf{F}$ as

$$J \equiv \left\langle \frac{dE}{dt} \right\rangle_t = \left\langle \sum_{\eta=1}^{N'} \mathbf{F}_\eta \cdot \dot{\mathbf{u}}_\eta \right\rangle_t, \tag{19}$$

where N' indicates the number of surface atoms in the lower body. If there is no viscous resistance due to the atmosphere and fluid around the sliding body, energy loss occurs solely at the interface; thus, the quantities J in Eqs. (18) and (19) are equal. There are two way for defining the kinetic friction coefficient: one is the division of friction force by the normal load and another is the thermodynamic definition in Eq. (18). Of course, the values of the friction coefficient from both definitions are the same. However, through Eqs. (18) and (19) using the SI-DLGF, the friction coefficient can be decomposed into the contributions of surface phonon modes and we can extract effective information about the relevance of the dynamics of surface atoms to friction.

For the following procedure, it is convenient to use the discrete Fourier transformed formulation. From the expression in the wave number l space, Eq. (19) can be written as

$$J/N' = \left\langle \sum_l \mathbf{F}_\mathbf{l}^* \cdot \dot{\mathbf{u}}_\mathbf{l} \right\rangle_t, \tag{20}$$

where $*$ indicates a complex conjugate. Then, substituting Eqs. (10) and (11) into Eq. (20) and denoting J_u as the energy dissipation components of vibrations in the x and z directions, we can obtain

$$J_u/N' = \langle \dot{u}^0 \rangle_t \bar{F}^u + \frac{1}{m}\sum_l |F_l^u(0)|^2 \mathrm{Re}\, s_l(0) + \frac{1}{2m}\sum_l \sum_{n=1}^{\infty} |F_l^u(\omega_n)|^2 \mathrm{Re}\, s_l(\omega_n),$$

where $\bar{F}^u$ is the averaged force per surface atom. $F_l^u(\omega_n)$ is a complex Fourier coefficient of $F_l^u(t)$ with a time period of T

$$F_l^u(\omega_n = 0) = \frac{1}{T}\int_{-T/2}^{T/2} F_l^u(t)dt,$$

$$F_l^u(\omega_n \neq 0) = \frac{2}{T}\int_{-T/2}^{T/2} \exp(i\omega_n t)F_l^u(t)dt,$$

where the vibration frequency $\omega_n=2\pi n/T$, $(n=1,2,\ldots)$. $s_l(\omega)$ is the Fourier-Laplace transformed form of $s_l(t)$ and it is given by

$$s_l(\omega) = \int_0^\infty \exp(-i\omega t)s_l(t)dt. \tag{21}$$

As shown in Appendix B, $s_l(\omega)$ can be derived analytically. In the case of $\beta_l^2 < (\omega/\alpha)^2 < \beta_l^2 + 1$, the calculation yields

$$\mathrm{Re}\, s_l(\omega) = \frac{2\omega}{\alpha^2}\sqrt{\frac{1}{(\omega/\alpha)^2 - \beta_l^2} - 1} \tag{22}$$

otherwise $\mathrm{Re}\, s_l(\omega) = 0$. Using this fact and $\langle \dot{u}^0 \rangle_t = -2\bar{F}^u/(\alpha m)$ in the steady state, which is derived by Eqs. (14) and (15), we obtain

$$J_u/N' = \frac{1}{2m}\sum_l \sum_{n=1}^{\infty} |F_l(\omega_n)|^2 \mathrm{Re}\, s_l(\omega_n). \tag{23}$$

Substituting Eq. (23) into Eq. (18), we can obtain

$$\mu = \sum_{u=x,z} \sum_l \sum_{n=1}^{\infty} \mu(u,l,\omega_n),$$

$$\mu(u,l,\omega_n) = \frac{1}{2m\bar{F}^z V}|F_l(\omega_n)|^2 \mathrm{Re}\, s_l(\omega_n), \tag{24}$$

where $\bar{F}^z = F_P/N'$ is the averaged normal force per surface atom. As can be seen in Eq. (24), the friction coefficient is decomposed by the surface phonon modes (u,l,ω_n). The index u indicates the contributions of the vibrations in the x and z directions: the transverse and longitudinal wave modes.

We note two interesting points from the above results. As seen in Eq. (24), the friction coefficient is written by the sum of the multiplications of the mode components of the surface interaction force $|F_l^u(\omega_n)|^2$ and the real part of the SI-DLGF $s_l(\omega)$. Because the SI-DLGF depicts the response of a solid considering the infinitely large bulk atoms, the friction coefficient is expressed separately as surface interaction $\times$ energy dissipation property of a solid in the mathematical form (rigorously, the surface interaction depends on the variable positions of the surface atoms, and thus, they are not completely independent). Thus, we recognize the need to treat not only the surface characters but also the mechanism of energy dissipation reflecting the bulk properties for the sliding friction, as mentioned in Sec. I.

Another important point is the energy absorption band corresponding to the wave number l mode. The real parts of s_l are plotted in Fig. 2. Re s_0 holds finite values in the frequency range from 0 to α. In the case of the $l \neq 0$ mode, Re $s_l(\omega)$ has finite values only in the range of $\beta_l^2 < (\omega/\alpha)^2 < \beta_l^2 + 1$. There exists a frequency band of energy absorption corresponding to wave number mode l and it does not absorb force components of frequencies that are not within the frequency band. We can also see a large peak around the low-frequency band edge $\omega = \alpha|\beta_l|$; it is attributed to vibration resonance. In other words, the l mode absorbs considerable energy from the force component corresponding to the resonant frequency.

III. COMPUTATIONAL DETAILS

We demonstrate the SI-DLGF method and the friction decomposition for two simple systems of solid friction: one is the friction between flat surfaces and the other is the friction between periodically contacting surfaces. Both are two-dimensional systems, and the upper and lower surfaces have an identical lattice constant.

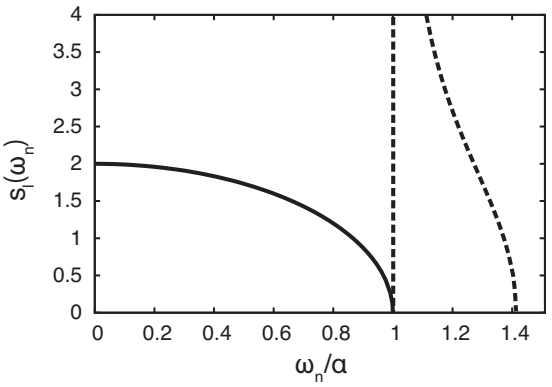

FIG. 2. Real parts of $s_l(\omega_n)$. Solid and dashed lines indicate Re s_0 and Re s_l at $\beta_l = 1.0$, respectively. Both lines are obtained with $\alpha = 1.0$.

We perform all simulations with the bulk parameters as those of diamond. The spring constants of diamond are estimated to be $K_x = K_z' = 0.1$ and $K_z = K_x' = 0.15$ a.u. using electronic state calculations based on the density-functional theory (DFT) employing the computational code Tokyo *ab initio* program package (TAPP).[54] The lattice distance is $\sigma = 2.88$ Bohr and the mass is set to that of a carbon atom. Because this study does not focus on specific features of the interaction force between surfaces, we use a simple but unrealistic force function. We employ the same soft-core potential as that used in our previous work,[46] in which an attractive potential is neglected as a first approximation. The cutoff radius of the potential is equivalent to the carbon diameter and the repulsion term is determined by fitting an sp^3 C-C bond repulsion caused by compressing the bond length, which is obtained by the DFT calculations. The specific force function is

$$F_\eta^u = 0.1\sum_a \left\{\left(\frac{\sigma}{r_a}\right)^6 - 1\right\}\frac{u_\eta - u_a}{r_a} H(\sigma - r_a),$$

where the index a represents the upper surface atoms and r_a is the distance between the upper and lower surface atoms. H is the Heaviside step function.

The time evolution of the atoms is obtained by the fourth-order Runge-Kutta method with an interval of a time step of 0.1 fs. The friction coefficient is calculated by dividing the time-averaged friction force by the normal force. The friction decomposition is performed in accordance with Eq. (24) through the Fourier transformation of the force trajectories.

In the SI-DLGF method, we set $t_c = 2.8$ ps, base number of the fast convolution $B = 10$, and number of points on Talbot's integral contour as 21. We confirmed that these parameters ensure reliable calculations. For a self-consistent scheme for a steady state, the efficient convergence of A_x^* is achieved by the time interval of each iteration set at σ/V, where V is the sliding velocity. The mixing parameter is ϵ

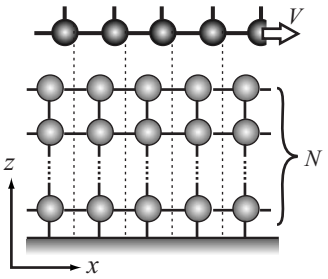

FIG. 3. Schematic image of the friction system between flat surfaces. The lower body is a coupled-oscillator surface model that consists of N inner bulk atomic layers. In the upper body, the atomic bonds are frozen at their equilibrium positions, and they slide at velocity V. The lattice constants of both bodies are the same.

=0.5. The iterations are performed until the error of the friction coefficient from the previous iteration is less than 1%.

The SI-DLGF method can couple with the direct calculation of the motion equation because it is originally based on the motion equation. We arrange one diamond-atomic layer connected to a layer described by the SI-DLGF method; in other words, the coupled motion equation is

$$m\ddot{u}_{\eta}^{\mathrm{ar}} + K_u(u_{\eta}^{\mathrm{ar}} - u_{\eta}) + K_u'\left(2u_{\eta}^{\mathrm{ar}} - \sum_{\Delta\eta} u_{\eta+\Delta\eta}^{\mathrm{ar}}\right) = F_{\eta}^{u},$$

where u^{ar} indicates the displacement of the arranged diamond-atomic layer. The counter reaction force of the elasticity $K_u(u_{\eta}^{\mathrm{ar}}-u_{\eta})$ is substituted into the force term in Eq. (9). The arranged layer, in turn, behaves as the surface atomic layer of the semi-infinite lattice system. Although the arrangement appears to be less meaningful for describing the semi-infinite system, it is numerically advantageous. The arranged layer corrects slight disagreements in the atomic displacements u_{η} that arise from the numerical error of the convolution in the SI-DLGF method.

Seeing friction dependence on the bulk layers clearly, we also perform calculations using a finite-slab surface model that consists of N atomic layers aligned in the z direction and introduce a velocity-proportional damping term. The artificial damping term should be determined so as to suitably reproduce the energy decay of a surface atom. We choose the damping term as $\sqrt{K_u m}\dot{u}_{\xi}/(N+1-\xi)$, and add it to the left-hand side of Eq. (1). The detailed derivation of the damping term is described in Appendix C. It is known that this way of introducing the damping terms, which act strongly on deeper bulk atoms, can prevent vibrational energy reflection at the bottom of the lower solid.[45]

IV. RESULTS AND DISCUSSIONS

A. Solid friction between flat surfaces

We consider a friction system in which the upper and lower bodies have a same lattice constant and atomically flat surfaces, as shown in Fig. 3. The atoms in the upper body are frozen at their equilibrium positions for simplicity and slide at 10 m/s. The lower body is modeled by coupled oscillators consisting of N atomic layers in depth and periodic boundary condition is applied in the x direction. Owing to the translation symmetry of the friction system, all the surface atoms are subjected to the same interaction force, and thus, the surface atoms move coherently. This is substantially equivalent to the one-dimensional chain model; thus, it allows to excite only the wave number $l=0$ mode of the surface phonon.

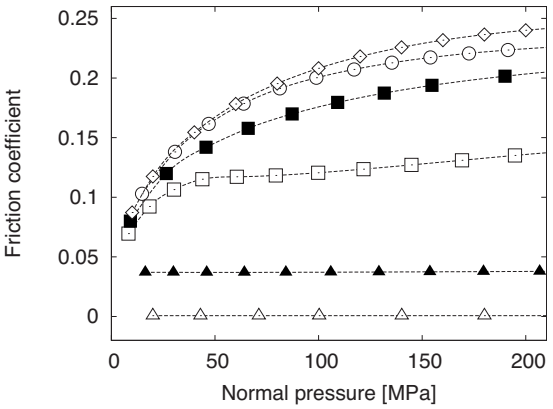

FIG. 4. Dependence of friction coefficient on the number of atomic layers N at a sliding speed of 10 m/s. △, ▲, □, ■, ○, and ◇ indicate friction coefficients for $N=1$, 100, 300, 1000, 2000, and ∞, respectively. The values with $N=\infty$ are obtained by the SI-DLGF method.

Figure 4 shows the dependence of friction coefficients on N. In the case of $N=1$, the friction coefficients are almost zero. On the other hand, the friction coefficients increase with N and the values converge to those of infinite N. The friction coefficients increase with a higher normal pressure in large N systems. This is because the interaction force we use does not include an attractive force, and the surface atoms of the upper and lower bodies bite deeper each other with a higher normal pressure; this is called the atomistic locking state.[55] It is also seen that over a thousand bulk atoms contribute to the friction coefficients. The result indicates the importance of including the bulk atoms for the analysis of the solid friction.

To clarify the role of the bulk atoms, the time variations of the force on the lower surface atoms are shown in Fig. 5. In the case of $N=1$, the force in the x direction is relatively small as compared to that in the z direction, and that in the x direction takes a sinusoidal profile with both plus and minus

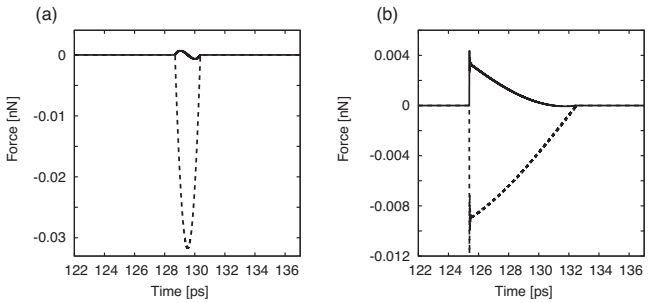

FIG. 5. Time histories of force on surface atoms of the lower bodies. (a) and (b) show the results of $N=1$ and ∞ surface models, respectively. Solid and dotted lines indicate forces in the x and z directions, respectively. Normal pressure is 100 MPa.

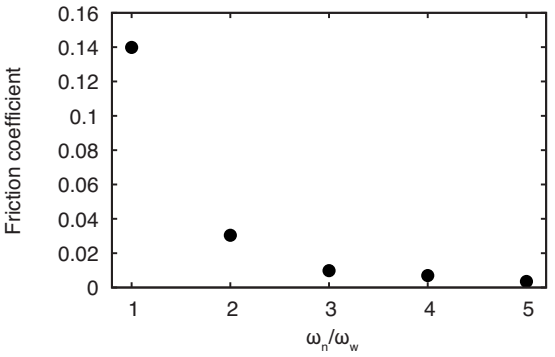

FIG. 6. Decomposition of friction coefficient with frequency ω_n modes. ω_w represents washboard frequency. Normal pressure is 100 MPa.

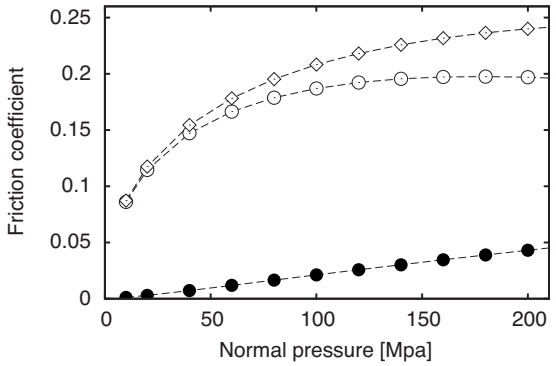

FIG. 7. Contributions of longitudinal (○) and transverse (●) wave modes to the total friction coefficient (◇).

values. On the other hand, in the $N=\infty$ system, the forces increase sharply when the surface atoms of both solids come into contact, and they decay slowly. The force shapes are not symmetrical and the force in the x direction maintains positive vales in total; namely, a friction force appears.

The $N=1$ system, equivalent to a harmonic oscillator, has one eigenresonance frequency $\alpha/2=\sqrt{K_u/m}$, and the oscillator resonates with the force component of the frequency. On the other hand, in terms of the interaction force, the eigenfrequency is regulated by the sliding velocity V and a lattice constant σ as

$$\omega_n = 2\pi nV/\sigma = n\omega_w,$$

where $n=1,\ldots,\infty$ and $\omega_w=2\pi V/\sigma$ that is called "washboard frequency." The washboard-frequency component often becomes the main term of the interaction force.[55] The eigenfrequency of the $N=1$ system is on the order of sound velocity, whereas ω_w is on the order of the sliding velocity below ~m/s in general. Thus, the harmonic oscillator does not resonate with the shear. The surface atoms change their positions adiabatically in response to changes of the interaction force. In this manner, the surface atoms experience both positive and negative friction forces, resulting in near-zero friction.

In the case of infinite N, on the other hand, the force in the x direction increases and finite values of the friction coefficient appear. This can be understood from the friction decomposition. Figure 6 shows the decomposition with the frequency modes. It is seen that the lowest frequency ω_w component shares a large amount with the total friction coefficient. The contributions of the higher frequency decrease. Namely, the surface phonon mode of ω_w generates the large energy dissipation of the friction system.

The friction dependence on N can be explained in terms of the concept of the energy absorption band. As N increases, the number of the eigenfrequency, ω_j^D in Sec. II B, increases. Consequently, as shown in Fig. 2, the energy absorption band ranging continuously $0<\omega_n<\alpha$ is formed in the limit of the infinite N system. The surface can absorb the low frequency of ω_w that is the main term of the interaction force, and thus, the friction occurs. It is also understood that over $N>1000$ atoms are required for the friction coefficient encompassing the resonance with ω_w because the characteristic frequency α is larger than ω_w by three orders of magnitude in the friction system.

Then, the friction contributions of the vibrations in the x and z directions, namely, the transverse and longitudinal wave modes, are shown in Fig. 7. The contribution of the longitudinal mode occupies a large share of the total friction coefficient. Because the ratio of the forces in the x and z directions, namely, friction coefficient, is below 0.25, the ratio of the frequency components of the forces in the x and z directions would also be of the same order. According to Eq. (24), the friction contribution is proportional to the square of the frequency component of the force. Therefore, the contribution of the longitudinal wave mode becomes large. This result indicates the importance of the degree of freedom of the z direction for the analysis of solid friction.

B. Solid friction between periodically contacting surfaces

Here we consider a friction system in which an upper surface periodically contacts with a flat lower surface, as shown in Fig. 8. In the unit cell, the lower body consists of infinite bulk atoms and the surface atoms of N' align along the x direction. In the upper body, the number of surface atoms is $N'/4$ in the unit cell, the intrabonds are frozen at their equilibrium positions, and the body slides at 10 m/s. To form the surface morphology, a periodic boundary condition

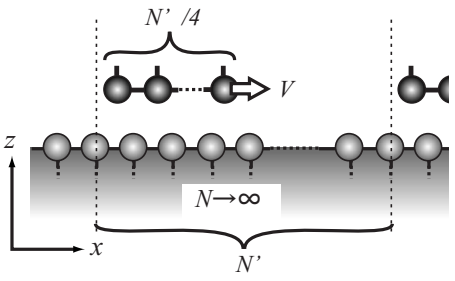

FIG. 8. Schematic image of the friction system with periodic contact areas. The lower body consists of infinitely large inner bulk atoms and N' surface atoms in a unit cell. The sliding upper body has $N'/4$ surface atoms in the unit cell and the atomic bonds are frozen. The lattice constants of the both bodies are the same. A periodic boundary condition applies to the unit cell.

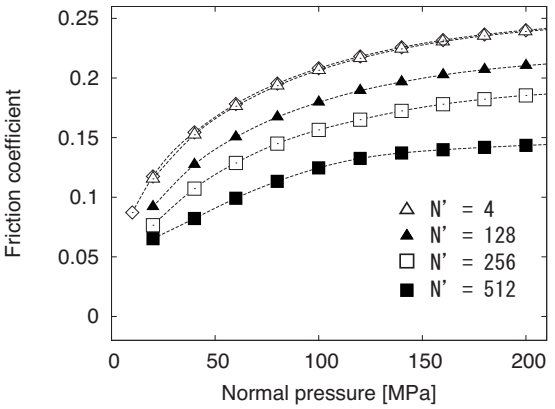

FIG. 9. Dependence of friction coefficient on N'. As a reference value, the friction coefficients for the friction system between flat surfaces are plotted by ◇ (same plot as that shown in Fig. 4).

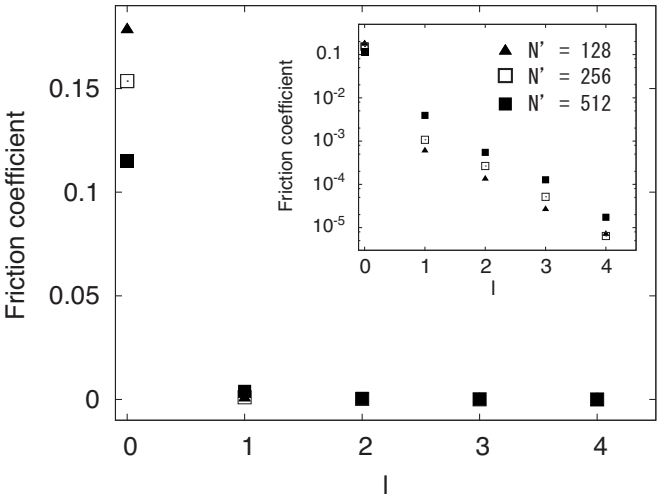

FIG. 10. Decomposition of friction coefficient with wave number l modes in the range of $l \geq 0$. Normal pressure is 100 MPa. The inset shows the same plot on a log scale.

is applied to the unit cell in the x direction. The normal force per surface atom does not change with the variation of N' at the same normal pressure because the ratio of the numbers of upper and lower surface atoms is fixed at 1/4. We assume that the lattice constants of both the bodies are same. Therefore, the condition of the contacting area is the same as that of the former friction system with the exception of the noncontacting area. Thus, the lower surface atoms are allowed to vibrate not only in the wave number $l=0$ mode but also in the $l \neq 0$ modes.

From the analysis of the friction system, the influence of the excitation of the $l \neq 0$ modes on friction should be clarified. Furthermore, there is another aspect to discuss the friction system. In actual solid friction, the surface is not completely flat but there exist many tiny protrusions on it and the protrusions contact the opposite surface producing friction.[2] Namely, because of coexisting real contact points and non contacting area on the real friction surface, the study of the friction system here also serves as a basic analysis of the real contact points.

Figure 9 shows the variations in the friction coefficients with an increase in N'. In the case of $N'=4$, the friction coefficients remain almost unchanged as compared to the values of the friction between flat surfaces. This can be understood from the energy absorption band of the surface phonon modes. The interaction force has the main term corresponding to the washboard frequency ω_w and the magnitude of the term at the higher frequency $\omega_n = n\omega_w$ decreases as n increases. On the other hand, the wave number l mode takes an energy absorption band ranging from $\beta_l^2 < (\omega_n/\alpha)^2 < \beta_l^2 + 1$. The characteristic frequency of the solid α is larger than ω_w by a factor of one thousand in this friction system. Therefore, the condition in which the energy absorption band absorbs the main force component of ω_w is roughly estimated by $10^3\pi|l| < N'$, where we approximate $\sqrt{K_u'/K_u} \sim 1$. Thus, a large N' is required to absorb the main component of the interaction force. When N' is much smaller, say, $N'=4$, $l \neq 0$ modes absorb only the higher frequency components of the force that are negligible amplitudes; and thus the coherent mode, $l=0$, accounts for the friction coefficient. Therefore, the $N'=4$ system has almost the same values as the system between flat surfaces.

However, with an increase in N', the friction coefficients decrease, as shown in Fig. 9. To analyze larger systems with $N'=128$, 256, and 512, the friction decompositions with the wave number l modes are shown in Fig. 10. The plots indicate the friction contributions of l modes, which are defined by the sum of Eq. (24) over frequencies as

$$\mu(l) = \sum_{n=1}^{\infty} \mu(x,l,\omega_n) + \mu(z,l,\omega_n). \tag{25}$$

Because $\mu(l) \sim \mu(-l)$ due to the symmetry of l, we show the values in the range of $l \geq 0$. As N' increases, the friction contributions of $l \neq 0$ modes increase, whereas that of the $l=0$ mode decreases. This is because the energy absorption bands of $l \neq 0$ modes shift to the lower frequency range, and thus, the absorbed lower frequency components of the interaction force increase. The reason for the decrease in the friction contribution of $l=0$ is explained as follows. The coherent movements of the surface atoms are impeded by the enhancement of the $l \neq 0$ modes. Accordingly, the coherent components of the interaction force decrease and this leads to the reduction in the friction contribution of $l=0$. Although the friction contributions of $l \neq 0$ increase, they do not absorb the main force term of ω_w and are thus small. On the other hand, the contribution of $l=0$ decreases considerably because it originally shares a large amount of the friction coefficient; thus, the total friction coefficients decrease as N' becomes large.

Here we introduce a long-wavelength approximation for exploring systems with much larger N'. As discussed before, the wave number l does not absorb less frequency than its lower frequency edge $\alpha|\beta_l|$ in the energy absorption band. In addition, the force components of the higher frequencies are small. Therefore, it is expected that the friction behavior does not essentially change even if we cut off l modes above a certain high wave number. Thus, we introduce a cut-off frequency $\omega_c = n_{cut}\omega_w$ and consider only l modes that absorb frequencies below the cut-off frequency; namely, only l

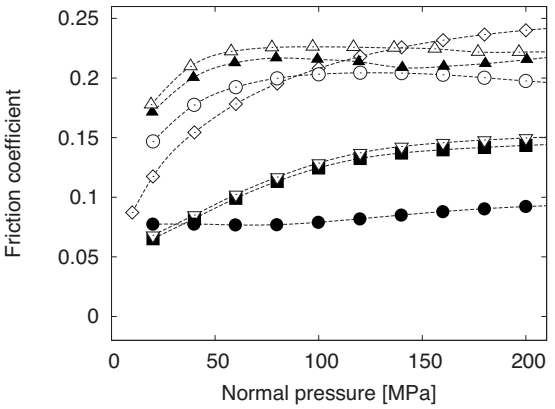

FIG. 11. Dependence of friction coefficient on N'. ▽, ●, ○, ▲, and △ indicate friction coefficients of $N'=512$, 1024, 2048, 8192, and 16 384 obtained by the long-wavelength approximation, respectively. As reference values, the friction coefficients for $N'=512$ without the long-wavelength approximation are indicated by ■ (same plot as that shown in Fig. 9) and the values for the system between flat surfaces are indicated by ◇ (same plot as that shown in Fig. 4).

modes that satisfy $\alpha|\beta_l|=2\sqrt{K'_u/m}|\sin \pi l/N'| < \omega_c$ are calculated in the simulations. Owing to the approximation, the calculation is sped up significantly. Figure 11 shows the friction coefficients obtained by the approximation with the parameter $n_{cut}=20$ and $K'_u=K'_x$. In the case of $N'=512$, the friction coefficients with the approximation (white inverted triangles) are slightly larger than those without the approximation (black squares). This is because the inhibition of the energy dissipation of $l=0$ is weakened owing to the $l\neq 0$ modes being cut off. However, the differences between the values are less than 5%, and thus, the approximation should be reasonably accurate for the friction system.

By applying the long-wavelength approximation, the friction coefficients of a much larger N' system are obtained. As shown in Fig. 11, the values decrease further in the $N'=1024$ system (black circles) and they increase suddenly in the $N'=2048$ system (white circles). As N' increases further, the values increase but at a lesser rate and the profiles become convergent.

In order to analyze the changes in the friction coefficients, they are decomposed by l modes. Figure 12 shows the profiles of $\mu(l)$ in the cases of $N'=1024$ and 2048. In $N'=2048$, a significant increase in the contributions at $|l|=1$ is clearly observed. The analysis of the energy absorption edge for $N'=2048$ suggests that this results from the $|l|=1$ modes absorbing the main force term of the ω_w component. In other wards, channels of the energy dissipation $|l|=0$ and 1 open, and consequently, the total friction coefficients suddenly increase. For $N'\geq 2048$, the energy dissipation channels that absorb the ω_w component successively open through the modes $|l|=0,1,2,\ldots$, and thus, the total friction coefficients increase.

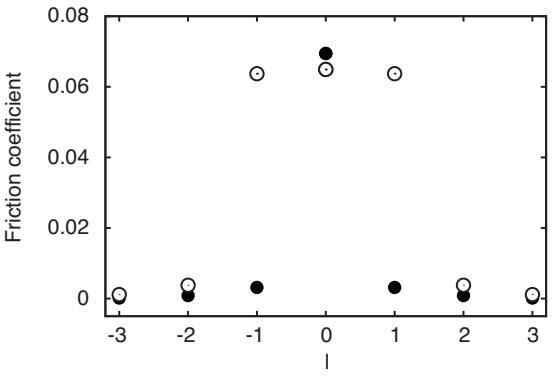

FIG. 12. Decomposition of friction coefficient with wave number l modes. ● and ○ indicate $\mu(l)$ for $N'=1024$ and 2048, respectively. Normal pressure is 100 MPa.

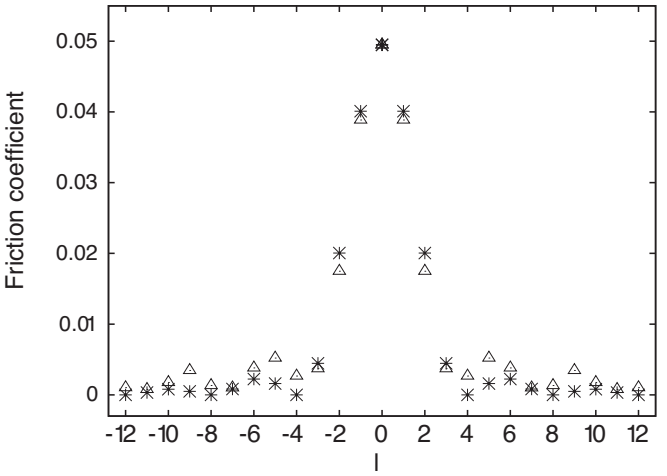

FIG. 13. Decomposition of friction coefficient with wave number l modes. △ indicate $\mu(l)$ for $N'=16\,384$. Asterisks indicate $\mu^*(l)$ that is derived with the continuum model [see Eq. (27) in the text]. Normal pressure is 100 MPa.

Although the friction coefficients increase with N', the values do not diverge but appear to converge. To obtain the insight into such a large N' system, the profile of $\mu(l)$ for $N'=16384$ is shown in Fig. 13 (white triangles). The friction contribution of $l=0$ is the largest and the value decreases with fluctuation as $|l|$ increases.

To understand the damped-vibration profile of $\mu(l)$, we consider a simple continuum model. First, the solids in the friction system shown in Fig. 8 are assumed as continuum bodies in the limit of large N'; the lengths of the upper and lower surface are L and ML, respectively, where M indicates the factor by which the lower surface is larger than the upper one; $M=4$ in the being considered system. f^u denotes the applied force distribution of the lower surface in the x and z directions per unit length. Then, a simple approximation for f^u is used. The lower surface is subjected to a force only in the contact area and this force is assumed to remain uniform with position in the contact area; that is, $f^u(x,\omega_n)=f^u(\omega_n)\{H(x)-H(L-x)\}$, where H is the Heaviside step function. Substituting $f^u(x,\omega_n)$ into the continuum limit of Eq. (11), we can derive

$$|F^u_{l\neq 0}(\omega_n)|^2=|F^u_{l=0}(\omega_n)|^2\left\{\frac{M}{\pi l}\sin(\pi l/M)\right\}^2, \qquad (26)$$

where $|F^u_{l=0}(\omega_n)|^2=|Lf^u(\omega_n)|^2$. Then, because of the large values of N', Re $s_l(\omega)\sim$ Re $s_0(\omega)$ according to Eq. (22). By the

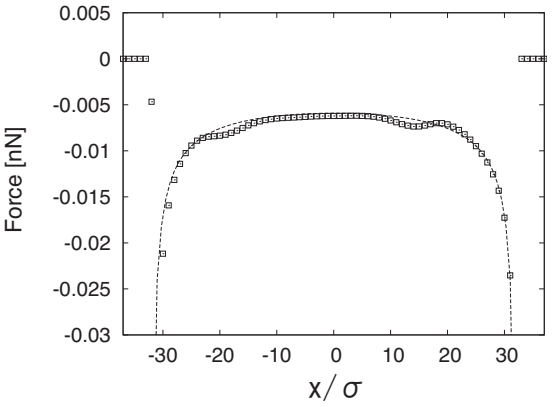

FIG. 14. Distribution of time-averaged force in the z direction on the lower surface atoms. The force is averaged over the time required by the upper body to slide one period of the lattice. Plots are those for $N'=256$ and the dashed line indicates the force distribution calculated by the theory of elastic contact. σ represents the lattice constant and normal pressure is 100 MPa.

approximation of the SI-DLGF, substitution of Eq. (26) into Eq. (24), and the use of Eq. (25), the friction decomposition of the l mode based on the continuum model can be written as

$$\mu^*(l \neq 0) = \mu(l=0)\left\{\frac{M}{\pi l}\sin(\pi l/M)\right\}^2. \tag{27}$$

Using the numerically obtained value of $\mu(l=0)$ in Eq. (27), the approximated $\mu^*(l)$ is obtained. $\mu^*(l)$ has zero nodes at l multiples of four corresponding to $M=4$, and the friction component is inversely proportional to the square of l. The values of $\mu^*(l)$ are replotted in Fig. 13 (asterisks). It is seen that $\mu^*(l)$ well describes the profile of $\mu(l)$. Thus, the damped-vibrational behavior of $\mu(l)$ is attributed to the ratio of the upper and lower areas and the expansion coefficients of the force with wave number.

In particular, at $|l|=9$, we can see that the friction contribution is much larger than the value expected by the continuum model. From the estimation of the energy absorption edge, we can see that the transverse wave at $|l|=9$ absorbs the ω_w component at its lower band edge and $|l|\geq 10$ does not absorb the ω_w component. As shown in Sec. II E, the real part of the SI-DLGF has a resonant peak around its lower frequency band edge. Thus, the transverse phonon mode of $|l|=9$ resonates with the interaction force driven by the shear and the energy dissipation due to the resonated mode is enhanced. As a result, the friction contribution is slightly larger than that obtained by the continuum model. To verify it, we performed a calculation for a system with $N'=32768$ (not shown here), and confirmed that the friction contribution of $|l|=9$ is much closer to the value expected by the continuum model because, in turn, the resonant peak is assigned at $|l|=18$.

Next, the applied force distribution on the lower surface atoms is considered. Figure 14 shows the distribution of the force in the z direction for the $N'=256$ system. The force is averaged over the time it takes the upper body to slide in one period of the lattice constant. This force has a large amplitude around the edge of the contact area and it decreases as being closer to the center of the area. According to the classical theory of elastic contact, in two-dimensional contact, when a rigid stamp with a flat bottom is pressed on an infinitely large elastic body, the normal force distribution is given by[3]

$$F(x) = \frac{\bar{f}^z L}{\pi\sqrt{(L/2)^2 - x^2}}, \tag{28}$$

where $\bar{f}^z$ denotes the averaged normal force in the z directions per unit length. There is no arbitrary fitting parameter in Eq. (28). The force distribution is replotted in Fig. 14. It exhibits good agreement with that obtained by our method although there is a small deviation because of the asymmetry in the x direction due to the sliding effect. In Fig. 13, the profile of $\mu(l)$ has peaks at slightly lower wave numbers than these expected by the simple continuum model and the friction contribution is not completely zero at l multiples of four. In the continuum model, to derive $\mu^*(l)$, we assumed uniformity of the contact force, although the actual force has the local distribution shown in Fig. 14. This accounts for the fact that the profile of $\mu(l)$ shifts to a lower wave number range and the values are not completely zero at the nodes. It is expected that if the local distribution of the force is included in the continuum model, a more accurate value of $\mu^*(l)$ would be obtained.

We note an interesting point through these results. Unless the order of N' is around 10^4, $\mu(l)$ does not exhibit good agreement with $\mu^*(l)$. Furthermore, as shown in Sec. IV A, the number of bulk layers required for solid friction is on the order of 10^3. Thus, our friction analysis includes tens of millions of atoms in total to obtain the friction property in the continuum limit. On the other hand, the force distribution of the contact area shows good agreement with that obtained by the classical theory of elastic contact for N' of the order of a few hundreds. In addition, a molecular dynamics simulation showed that the force distribution agrees with the theory of elastic contact from the calculation of tens of thousands of atoms for such a two-dimensional contact between atomic-scale flat bodies.[19] This suggests that for a macroscopic system in which the continuum limit is effective, much larger atomistic degrees of freedom are required for the kinetic solid friction as compared to a static physical quantity such as force. Such a requirement of a large number of degrees of freedom might be one of the difficulties that have impeded the construction of a macroscopic approach for the solid friction starting from the atomistic theory.

Finally, we present overviews of the friction decompositions of the $N'=16384$ system mapped in the (l,ω_n) space for the transverse and longitudinal waves in Figs. 15(a) and 15(b), respectively. It is globally seen that from the main term of $(l=0,\omega_w)$, the friction contribution decreases with an higher frequency and it behaves as a damped vibration. Specifically, the transverse $(l=9,\omega_w)$ mode provides a relatively large contribution of the friction owing to the resonance of the surface phonon. Similarly, although the contribution of the longitudinal $(l=12,\omega_w)$ mode corresponds to the zero node expected by the continuum model we used, it has a

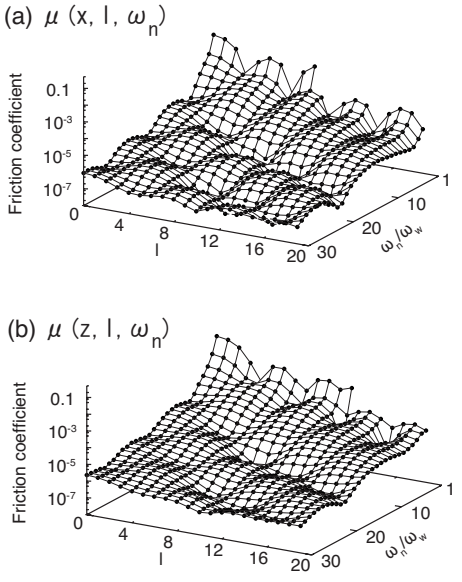

FIG. 15. Decomposition of friction coefficient with (u,l,ω_n) modes. (a) and (b) show the contributions of transverse and longitudinal modes to the friction coefficient for $N'=16\,384$, respectively. Normal pressure is 100 MPa.

large value owing to the resonance not to be the node. It can also be seen that the contributions of the longitudinal modes are larger than those of the transverse modes. In fact, the contributions of the longitudinal modes share approximately 70% of the total friction coefficient, and thus, the importance of the z degree of freedom is also confirmed in the friction system. As seen from the above results, the friction decomposition with surface phonon modes would be an effective tool for the analysis of solid friction, revealing a relationship between the dynamic process of surface atoms and energy dissipation.

V. SUMMARY AND CONCLUSION

In summary, we have developed the SI-DLGF method to incorporate the mechanism of energy dissipation due to phonon. The actual value of the SI-DLGF can be obtained by combining the analytically derived asymptotic solution of the SI-DLGF and the numerically obtained one based on the integral expression. A scheme to achieve a steady state in the friction systems is also presented. Using the analyticity of the SI-DLGF, we introduced a fast convolution method that significantly accelerates computation speed of the method. Focusing on energy dissipation rate, we presented the decomposition of the friction coefficient with surface phonon modes. It was also found that wave number l mode has an energy absorption band and the mode can absorb energy through the force term of frequencies only within the band.

These methods were demonstrated using simple friction systems between two-dimensional solids having identical lattice constants. One is the friction between atomically flat surfaces and the other is the friction between periodically contacting surfaces. The main results are listed in below: (a) energy dissipation occurs due to the excitation of surface phonons in the presence of bulk atoms. The surface phonon absorbs the main force term at the lowest frequency, i.e., washboard frequency ω_w. (b) Friction coefficient depends on size of the contact area. (c) When $l\neq 0$ modes do not absorb the force term of ω_w, the friction coefficient decreases. The $l\neq 0$ modes absorb faint force terms of frequencies higher than ω_w, and the $l\neq 0$ modes perturb the excitation of the $l=0$ mode that originally causes large energy dissipation. (d) When the contact size is so large that a sufficient number of $l\neq 0$ modes absorb the ω_w term, the friction coefficient increases. The profile of the friction decomposition with l modes exhibits good agreement with that estimated by a simple continuum model.

It is important to stress here that the values of friction coefficients in this paper were obtained in the commensurate systems. Friction generally occurs between incommensurate surfaces, and it is known that direct excitations of surface phonons by collision of surface atoms, namely, elastic instability, would be small.[51,52] Therefore, the simplicity we used does not allow to make prediction of actual experiments of friction that involves the interface phenomena such as plastic deformation, adhesion and wear.[21–24] Nevertheless, the virtue of the SI-DLGF method lies on its potential to depict dynamical response of solid surface and, equivalently, energy dissipation due to phonon. By this method combined with ordinal MD method, one might capture some important features of actual friction including heat transfer by phonon correctly. In addition, besides friction analysis, this method could be used to study dynamical contact mechanics such as effect of shear stress and surface deformation when the asperities collide, that cannot be treated by the static LGF approach.[12,42]

We comment on extensions of the SI-DLGF method. We treated two-dimensional coupled oscillators in which the structure is restricted to a square one, the intra-atomic bonds are replaced with springs connected to only the nearest neighbors and they are set at zero Kelvin. It can be readily extended to the three-dimensional structure through the analogous procedure. The introduction of a finite temperature has already been promised by the Adelman and Doll's[33,34] works within the framework of the generalized Langevin equation.[35,36] The extensions of a general structure and beyond the nearest-neighbor bond remain difficult at this stage. We feel that combining the asymptotic solution of our SI-DLGF with some numerical methods[37–41] might enable such extensions.

In this work, ten million order of atoms were treated substantially for the analysis of the solid friction. This is a great advantage of the SI-DLGF method because if one study such a large-scale system by an ordinary MD simulation, it may be laborious to obtain only one value of the friction coefficient even by using latest high-performance computers. In addition, it should be noted that a simple continuum-solid model could explain the friction decomposition with l modes in the large-scale system, although the actual value of the friction coefficient cannot be expected yet. This fact possibly helps to approach a macroscopic theory of solid friction starting from a microscopic approach.

The SI-DLGF method and the friction decomposition with surface phonon modes provide clear information about

the relationship between surface phonons and solid friction. From a different viewpoint, it appears to capture solid friction using the terminology of solid-states physics. Actually, the concepts of the decomposition with modes and the energy absorption band are commonly used such as electronic band structure, optical spectrum, and vibration spectrum.[56,57] These have greatly contributed to the development of fields such as electronic devices and surface science. In solid friction, these concepts have yet been adequately developed. We hope that the generalization of the SI-DLGF and the friction decomposition methods and the basic knowledge yielded by them will assist further developments of friction-control techniques.

ACKNOWLEDGMENTS

We would like to thank R. Kobayashi, S. Ogata, M. Tohyama, S. Sanda, and T. Yamada for their helpful discussions and comments.

APPENDIX A: ASYMPTOTIC SOLUTION OF SI-DLGF

After the Taylor expansion with t and performing the θ integral of Eq. (7), we obtain

$$s_l(t) = \sum_{n=0}^{\infty} \frac{(-1)^n}{(2n)!}(\alpha t)^{2n} \sum_{m=0}^{n} {}_nC_m \frac{2m!}{m!(m+1)!2^{2m}} \beta_l^{2(n-m)},$$

where ${}_nC_m$ indicates the number of combinations and it is defined as ${}_nC_m = n!/m!(n-m)!$ Changing the index $k=n-m$ and the order of the sum, we can decompose s_l as

$$s_l(t) = \sum_{k=0}^{\infty} s_l^k(t), \tag{A1}$$

$$s_l^k(t) = \frac{4^k}{k!}\beta_l^{2k} \sum_{n=k}^{\infty} \frac{(-1)^n n!\{2(n-k)\}!}{2n!\{(n-k)!\}^2(n-k+1)!} y^{2n},$$

where $y=\alpha t/2$. Then, s_l^k is expressed with $n'=n-k$ as

$$s_l^k(t) = \frac{(-2)^k}{k!}\beta_l^{2k} \sum_{n'=0}^{\infty} \frac{(-1)^{n'}}{n'!(n'+1)!} \times \frac{(2n'-1)!!}{(2n'+2k-1)!!} y^{2(n'+k)},$$

where we denote $n'!!=n'(n'-2)\cdots 3\cdot 1$ in the case of odd n' and $n'!!=n'(n'-2)\cdots 4\cdot 2$ in the case of even n'. Considering the forms of s_l^k and s_l^{k-1}, it is found that they satisfy the recurrence equation as

$$s_l^k(t) = \frac{-2}{k}\beta_l^2 y \int_0^y s_l^{k-1}(t)dy. \tag{A2}$$

Thus, s_l^k can be obtained by the recursive substitution of s_l^{k-1} in Eq. (A2). The first term s_l^0 does not depend on l and is equivalent to s_0; it can be expressed using the integral formula of the Bessel function as

$$s_0(t) = J_1(2y)/y.$$

$s_{l\neq 0}$ can be derived if we perform the sum in Eq. (A1). However, we could not perform the sum over infinite k. Thus, we focus on the large t region. s_l^1 is written as

$$s_l^1(t) = -2\beta_l^2 y \int_0^y dy J_1(2y)/y.$$

When y is sufficiently large, $\int_0^y dy J_1(2y)/y \to 1$, and thus, the asymptotic solution $\tilde{s}_l^1 = -2\beta_l^2 y$. Using Eq. (A2), we obtain

$$\tilde{s}_l^k(t) = 2\beta_l \frac{(-1)^k}{k!(k-1)!}(\beta_l y)^{2k-1}.$$

Therefore, the asymptotic solution of s_l can be obtained as

$$\tilde{s}_l(t) = s_0(t) + \sum_{k=1}^{\infty} \tilde{s}_l^k(t) = s_0(t) - 2\beta_l J_1(\alpha\beta_l t),$$

where the integral formula of the Bessel function was used again. Furthermore, the first term s_0 decays as $t^{-3/2}$; on the other hand, the second term slowly decays as $t^{-1/2}$. Thus, we can omit the first term as the asymptotic solution and derive

$$\tilde{s}_l(t) = -2\beta_l J_1(\alpha\beta_l t).$$

APPENDIX B: FOURIER TRANSFORMED SI-DLGF

By substituting Eq. (7) and performing the time integral, Eq. (21) can be written as

$$s_l(\omega) = \frac{4i\omega}{\pi\alpha^2} \int_{\beta_l}^{\sqrt{\beta_l^2+1}} \sqrt{\frac{1+\beta_l^2-X^2}{X^2-\beta_l^2}} \frac{X}{X^2-(\omega/\alpha)^2} dX,$$

where $X^2 = \sqrt{\sin^2\theta + \beta_l^2}$. Then, changing the variable $Y = \sqrt{(1+\beta_l^2-X^2)/(X^2-\beta_l^2)}$ and $A_l = 1+\{\beta_l^2-(\omega/\alpha)^2\}^{-1}$, the integral can be expressed as

$$s_l(\omega) = -\frac{4i\omega}{\pi\alpha^2} \int_0^{\infty} \left(\frac{1}{Y^2+1} - \frac{A_l}{Y^2+A_l} \right) dY.$$

Here we use an integral formula $\int_0^{\infty}(Y^2+A_l)^{-1} = \pi/(2\sqrt{A_l})$ and obtain

$$s_l(\omega) = \frac{2\omega}{\alpha^2} \left\{ \sqrt{\frac{1}{(\omega/\alpha)^2-\beta_l^2}} - 1 - i \right\}.$$

APPENDIX C: FINITE-SLAB SURFACE MODEL

In a finite slab model that consists of N atomic layers, an energy damping term has to be set in the motion equation because it becomes an energy-conserving system without damping. The purpose of this appendix is to derive a suitable damping term so as to reproduce the energy dissipation of the vibration wave generated by sliding. As a reference system, we consider the one-dimensional chain system in which the surface atom is distorted initially.

$$\ddot{u}_\xi + \frac{K_u}{m}\left(2u_\xi - \sum_{\Delta\xi} u_{\xi+\Delta\xi} - \delta_{\xi,1} u_1^0 \right) = 0, \tag{C1}$$

$$u_\xi^0(t=0) = X\delta_{\xi,1}, \quad \dot{u}_\xi^0(t=0) = 0.$$

The motion of equation can be solved by a procedure similar to that shown in Sec. II C.

$$u_\xi(t) = \frac{2X}{2N+1}\sum_{j=1}^{N}\{\cos[\pi(2j-1)\xi/(2N+1)] + \cos[\pi(2j-1)(\xi-1)/(2N+1)]\}\cos\omega_j^D t.$$

In the limit of $N\to\infty$, the position of the surface atom ($\xi=1$) is written as

$$u_1(t) = \frac{2X}{\sqrt{\alpha t}}J_1(\alpha t). \tag{C2}$$

Then, we determine the damping term relative to the infinite N solution. We assume that the damping term is proportional to the atomic velocity. Owing to the dimension analysis of Eq. (C1), the damping term should be $\mathcal{C}_\xi\sqrt{K_u m}\dot{u}_\xi$, where $\mathcal{C}_\xi$ is a dimensionless parameter. We choose $\mathcal{C}_\xi = \mathcal{C}/(N+1-\xi)$ and $\mathcal{C}=1.0$. The damping term we use is chosen to increase as deeper bulk atoms. We have confirmed that this prevents a reflected wave rather than simply using a constant damping term.

Figure 16 shows the surface positions obtained by the numerical calculation of the motion equation including the damping term and the infinite N solution of Eq. (C2). As shown in Fig. 16(a), in the case of $N=40$, the damping profile of the surface atom is very close to that of the infinite N system. On the other hand, in the case of $N=1$, the damping profile differs considerably from that of the infinite N system; although we tried several values of $\mathcal{C}$, the results did not change greatly. Figure 16(b) shows the profiles at a time when a vibration wave that results from the initially given displacement of the surface returns to the surface. While the profile without the damping term recovers its amplitude that with the damping term suppresses the reflected wave as in the case of the infinite-N profile. These results indicate that the damping term we chose is expected to mimic the energy dissipation due to phonon well.

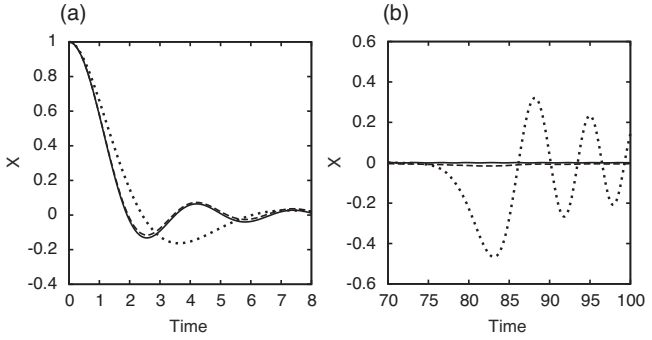

FIG. 16. Profiles of the surface positions. (a) Solid line, dashed line, and dotted line indicate the surface-atomic positions in the $N\to\infty$ [Eq. (C2)], $N=40$, and $N=1$ systems, respectively. The finite systems include the damping term described in the text. (b) Solid line, dashed line, and dotted line indicate the surface-atomic positions in the $N\to\infty$, $N=40$ with and without the damping term, respectively.

[1] D. Dowson, *History of Tribology* (Longman, London, 1979).
[2] F. P. Bowden and D. Tabor, *The Friction and Lubrication of Solids* (Clarendon Press, Oxford, 1954).
[3] L. A. Galin, *Contact Problems in the Theory of Elasticity* (North Carolina State College, North Carolina, 1961).
[4] A. Cameron, *The Principles of Lubriction* (Longman, London, 1966).
[5] D. Dowson and G. R. Higginson, *Elasto-Hydrodynamic Lubrication* (Pergamon Press, Oxford, 1977).
[6] J. A. Greenwood and J. B. P. Williamson, Proc. R. Soc. London, Ser. A **295**, 300 (1966).
[7] M. Ciavarella, J. A. Greenwood, and M. Paggi, Wear **265**, 729 (2008).
[8] B. N. J. Persson, J. Chem. Phys. **115**, 3840 (2001).
[9] B. N. J. Persson, Phys. Rev. Lett. **99**, 125502 (2007).
[10] T. Nakahara and S. Momozono, Proceedings of the Institution of Mechanical Engineers, Part J: Journal of Engineering Tribology **222**, 335 (2008).
[11] L. Pei, S. Hyun, J. F. Molinari, and M. O. Robbins, J. Mech. Phys. Solids **53**, 2385 (2005).
[12] C. Campañá, M. H. Müser, and M. O. Robbins, J. Phys. Condens. Matter **20**, 354013 (2008).
[13] B. N. J. Persson, *Sliding Friction: Physical Principles and Application*, 2nd ed. (Springer, Berlin, 2000).
[14] C. M. Mate, *Tribology on the Small Scale* (Oxford University Press, New York, 2008).
[15] S. Sasa and H. Tasaki, J. Stat. Phys. **125**, 125 (2006).
[16] M. Ishikawa, R. Harada, N. Sasaki, and K. Miura, Phys. Rev. B **80**, 193406 (2009).
[17] Y. Mo and I. Szlufarska, Phys. Rev. B **81**, 035405 (2010).
[18] G. He, M. H. Müser, and M. O. Robbins, Science **284**, 1650 (1999).
[19] B. Luan and M. O. Robbins, Nature (London) **435**, 929 (2005).
[20] S. Cheng, B. Luan, and M. O. Robbins, Phys. Rev. E **81**, 016102 (2010).
[21] C. Campañá, Phys. Rev. B **75**, 155419 (2007).
[22] M. H. Müser, Tribol. Lett. **10**, 15 (2001).
[23] B. L. Holian and J. E. Hammerberg, Phys. Rev. E **68**, 036101 (2003).
[24] D. K. Ward, D. Farkas, J. Lian, W. A. Curtin, J. Wang, K.-S. Kim, and Y. Qi, Proc. Natl. Acad. Sci. U.S.A. **106**, 9580 (2009).
[25] M. Chandross, C. D. Lorenz, M. J. Stevens, and G. S. Grest, Langmuir **24**, 1240 (2008).
[26] H. Washizu, S. Sanda, S. Hyodo, T. Ohmori, N. Nishino, and A. Suzuki, SAE Trans., J. Mater. Manuf. **116**, 414 (2007).
[27] H. Washizu and T. Ohmori, Lubr. Sci. **22**, 323 (2010).
[28] N. Sasaki, N. Itamura, and K. Miura, Jpn. J. Appl. Phys., Part 2 **46**, L1237 (2007).
[29] S. Dag and S. Ciraci, Phys. Rev. B **70**, 241401(R) (2004).
[30] H. Mori, Prog. Theor. Phys. **33**, 423 (1965).
[31] R. Kubo, Rep. Prog. Phys. **29**, 255 (1966).
[32] R. Zwanzig, J. Chem. Phys. **32**, 1173 (1960).
[33] S. A. Adelman and J. D. Doll, J. Chem. Phys. **61**, 4242 (1974).
[34] S. A. Adelman and J. D. Doll, J. Chem. Phys. **64**, 2375 (1976).

[35] L. Kantorovich, Phys. Rev. B **78**, 094304 (2008).
[36] L. Kantorovich and N. Rompotis, Phys. Rev. B **78**, 094305 (2008).
[37] A. J. Chorin, O. H. Hald, and R. Kupferman, Proc. Natl. Acad. Sci. U.S.A. **97**, 2968 (2000).
[38] W. Cai, M. de Koning, V. V. Bulatov, and S. Yip, Phys. Rev. Lett. **85**, 3213 (2000).
[39] X. Li and W. E, Phys. Rev. B **76**, 104107 (2007).
[40] G. J. Wagner and W. K. Liu, J. Comput. Phys. **190**, 249 (2003).
[41] H. S. Park, E. G. Karpov, P. A. Klein, and W. K. Liu, J. Comput. Phys. **207**, 588 (2005).
[42] C. Campañá and M. H. Müser, Phys. Rev. B **74**, 075420 (2006).
[43] J. B. Sokoloff, Phys. Rev. B **42**, 760 (1990).
[44] J. B. Sokoloff, J. Appl. Phys. **72**, 1262 (1992).
[45] O. M. Braun, M. Peyrard, V. Bortolani, A. Franchini, and A. Vanossi, Phys. Rev. E **72**, 056116 (2005).
[46] S. Kajita, H. Washizu, and T. Ohmori, EPL **87**, 66002 (2009).
[47] C. Lubich and A. Schädle, SIAM J. Sci. Comput. (USA) **24**, 161 (2002).
[48] A. Talbot, J. Inst. Math. Appl. **23**, 97 (1979).
[49] G. Capobianco, D. Conte, I. D. Prete, and E. Russo, BIT **47**, 259 (2007).
[50] I. D. Prete, Ph.D. thesis, Università degli Studi di Napoli Federico II, 2006.
[51] M. Hirano and K. Shinjo, Phys. Rev. B **41**, 11837 (1990).
[52] K. Shinjo and M. Hirano, Surf. Sci. **283**, 473 (1993).
[53] M. H. Müser, EPL **66**, 97 (2004).
[54] J. Yamauchi, M. Tsukada, S. Watanabe, and O. Sugino, Phys. Rev. B **54**, 5586 (1996).
[55] M. Hirano, Surf. Sci. Rep. **60**, 159 (2006).
[56] J. M. Ziman, *Principles of the Theory of Solids*, 2nd ed. (Cambridge University Press, Cambridge, 1972).
[57] G. Attard and C. Barnes, *Surfaces* (Oxford University Press, New York, 1998).